

Rescattering effects in hadron-nucleus and heavy-ion collisions

Jianwei Qiu¹

Department of Physics and Astronomy, Iowa State University, Ames, Iowa 50011, U.S.A.

Received: October 26, 2018

Abstract. We review the extension of the factorization formalism of perturbative QCD to *coherent* soft rescattering associated with hard scattering in high energy nuclear collisions. We emphasize the ability to quantify high order corrections and the predictive power of factorization approach in terms of universal nonperturbative matrix elements. Although coherent rescattering effects are power suppressed by hard scales of the scattering, they are enhanced by the nuclear size and could play an important role in understanding the novel nuclear dependence observed in high energy nuclear collisions.

PACS. 12.38.Bx – 12.39.St – 24.85.+p

1 Introduction

Rescattering in hadron-nucleus and heavy-ion collisions provides an excellent tool to diagnose properties of nuclear medium and could play an important role in understanding novel nuclear dependence recently observed at relativistic heavy ion collider (RHIC) and in planning future experiments at the Large Hadron Collider (LHC). Many approaches in studying the rescattering effects have been proposed and used for calculating nuclear dependence in high energy nuclear collisions [1, 2, 3, 4, 5, 6, 7].

In this talk, we focus on a treatment of *coherent* soft rescattering associated with hard probes [2, 3]. Our work is based on perturbative QCD (pQCD) factorization approach, which is different from the works of Baier *et al.* (BDMPS) [4] and Zakharov [5], and the reaction operator approach of Gyulassy *et al.* [6]. The BDMPS analysis does not require the presence of a hard scattering, but describes the coherent results of many soft scatterings. Its primary subject is induced energy loss. Our analysis requires a hard scale, and begins with the pQCD treatment of hard-scattering with emphases on momentum transfer, caused by coherent initial- and final-state soft scatterings [2, 3]. Our work attempts to stay as close as possible to the pQCD factorization formalism, in which we may readily quantify high order corrections in powers of strong coupling constant α_s , as well as corrections that decrease with extra powers of momentum transfer [8, 9, 10, 11].

In the following we consider only initial- and final-state interaction that gives leading power in medium length ($A^{1/3}$) and in α_s at each scattering. We first identify the coherence length in nuclear collisions and the source of the leading medium size enhancement. We then apply pQCD factorization approach to calculate the leading nuclear dependence in several physical observables. We show that if we neglect soft rescattering off quark fields [12, 13], the

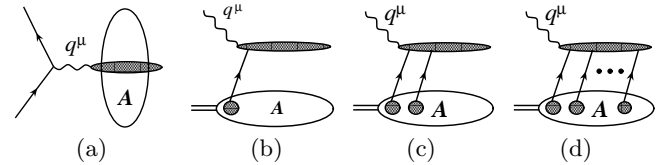


Fig. 1. Sketch for the scattering of a parton (or a lepton) in a large nucleus with a momentum transfer q^μ .

leading medium effects induced by multiple soft rescattering depend on only one well-defined nonperturbative matrix element, $\langle F^{+\alpha} F_{\alpha}^+ \rangle$, defined below. We extract its value from different physical measurements and discuss its universality. A brief summary is given at the end.

2 Coherent multiple scattering and leading nuclear A -dependence

A hard probe corresponds to a scattering process with a large momentum exchange q^μ whose invariant mass $Q \equiv \sqrt{q^2} \gg \Lambda_{\text{QCD}}$, as sketched in Fig. 1. It can probe a space-time dimension much smaller than a nucleon *at rest*, $1/Q \ll 2R \sim \text{fm}$, with nucleon radius R . But, the same probe might cover a whole Lorentz contracted large nucleus, if $1/Q > 2R(m/p)$ with averaged nucleon momentum p and mass m , or equivalently, $x \ll x_c \equiv 1/2mR \sim 0.1$ with x being an active parton momentum fraction in the scattering, $xp \sim Q$. The critical value x_c corresponds to the nucleon size. If the active x is much smaller than x_c , a hard probe could cover several nucleons in a Lorentz contracted large nucleus and interact with partons from different nucleons *coherently*.

Inclusive deeply inelastic scattering (DIS) on a nucleus offers an ideal example of coherent multiple scattering

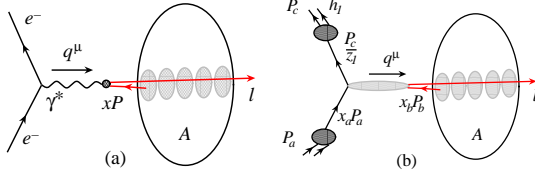


Fig. 2. Coherent multiple scattering of the struck parton in deeply inelastic scattering (a) and in t -channel in hadron-nucleus collisions (b).

and power corrections [11]. The strength of the scattering is defined by the virtual photon momentum, q^μ . Let $q^\mu = -x_B p^\mu + Q^2/(2x_B p \cdot n)n^\mu$ with n^μ defined along a lightcone direction opposite to that of p^μ . While the $Q^2 = -q^2$ sets up the hard collision scale, the scattered quark probes the nuclear matter via multiple soft final-state interactions. When Bjorken $x_B \equiv Q^2/2p \cdot q \ll x_c$, the multiple scatterings at a given impact parameter are coherent over entire size of the Lorentz contracted nucleus. This is best seen in the Breit frame, as shown in Fig. 2(a), where the incoming quark reverses its direction after interacting with the virtual photon and collides with the “remnants” of the nucleus at the same impact parameter. The same coherent multiple scatterings can take place in hadron-nucleus collisions along the direction of momentum exchange of the scattering [14], as shown in Fig. 2(b).

To identify the leading medium length enhanced nuclear effects, let's consider multiple scattering contribution to inclusive DIS off a large nucleus, as sketched in Fig. 2(a). For a spin-averaged inclusive DIS cross section, there is only one large momentum scale, Q , “invariant mass” of the exchanged virtual photon, and the factorization is expected to be valid for all power corrections as a consequence of operator product expansion (OPE) [15]:

$$\begin{aligned} d\sigma_{\text{DIS}}^{\gamma^*A} &= d\hat{\sigma}_2^i \otimes \left[1 + c^{(1,2)}\alpha_s + c^{(2,2)}\alpha_s^2 + \dots \right] \otimes T_2^{i/A} \\ &+ \frac{d\hat{\sigma}_4^i}{Q^2} \otimes \left[1 + c^{(1,4)}\alpha_s + c^{(2,4)}\alpha_s^2 + \dots \right] \otimes T_4^{i/A} \\ &+ \frac{d\hat{\sigma}_6^i}{Q^4} \otimes \left[1 + c^{(1,6)}\alpha_s + c^{(2,6)}\alpha_s^2 + \dots \right] \otimes T_6^{i/A} \\ &+ \dots \end{aligned} \quad (1)$$

where \otimes represents convolutions in fractional momenta carried by partons and T_n represents a parton correlation function or a matrix element of a twist n operator. In Eq. (1), the $\hat{\sigma}_n^i$ and $c^{(j,n)}$ are perturbatively calculable short-distance partonic cross sections or coefficient functions, which are independent of the target size. Therefore, we need to find the nuclear size ($A^{1/3}$ -type) enhancement induced by multiple rescattering from the matrix elements, if there is any.

The leading twist parton distributions, T_2 's, represent probability densities to find a single parton in a target and can have some nuclear dependence via the input distributions to their DGLAP evolution equations. The $A^{1/3}$ -type

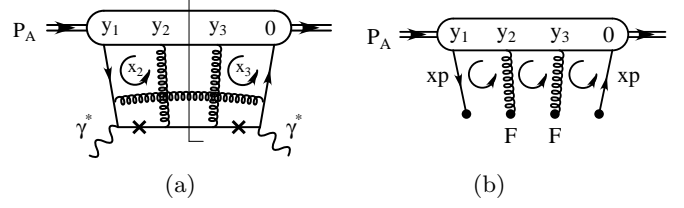


Fig. 3. (a) Diagram with poles that give rise to an $A^{1/3}$ -type enhancement to DIS cross section off a large nucleus; and (b) corresponding twist-4 quark-gluon correlation function.

target-size enhancement to DIS cross section can only appear in the terms beyond the first row in Eq. (1). For definiteness, let's consider a leading power suppressed contribution to DIS cross section, as shown in Fig. 3(a), which can be factorized into the form according to Eq. (1) [2],

$$\begin{aligned} d\sigma_A^{(4)} &= \sum_{(ii')} \int dx_1 dx_2 dx_3 T_{(ii')/p_A}^{(4)}(x_1, x_2, x_3) \\ &\times d\hat{\sigma}_{(ii')}^{(4)}(x_1, x_2, x_3). \end{aligned} \quad (2)$$

The matrix element $T^{(4)}$, as sketched in Fig. 3(b), is typically of the form [8],

$$\begin{aligned} T_{(ii')/p_A}(x_1, x_2, x_3) &\propto \int \frac{dy_1^- dy_2^- dy_3^-}{(2\pi)^3} e^{ip^+(x_1 y_1^- + x_2 y_2^- + x_3 y_3^-)} \\ &\times \langle p_A | B_i^\dagger(0) B_{i'}^\dagger(y_3^-) B_{i'}(y_2^-) B_i(y_1^-) | p_A \rangle, \end{aligned} \quad (3)$$

where $p = p_A/A$ and B_i is the field corresponding to a parton of type $i = q, \bar{q}, G$. The structure of the target is manifest only in the matrix element T in Eq. (2). Each pair of fields in the matrix element Eq. (3) represents a parton that participates in the hard scattering. The y_i^- integrals cover the distance between the positions of these particles along the path of the outgoing scattered quark. In Eq. (3), integrals over the distances y_i^- generally cannot grow with the size of the target because of oscillations from the exponential factors $e^{ip^+ x_i y_i^-}$.

Since the kinematics of a single-scale hard collision is only sensitive to the total momentum from the target, two of the three momentum fractions: x_1, x_2 , and x_3 cannot be fixed by the hard collisions. Therefore, there is always a subset of Feynman diagrams, like one in Fig. 3(a) with poles labeled by the crosses “ \times ”, whose contribution to the partonic parts, $\hat{\sigma}_{(ii')}^{(4)}$ in Eq. (2) is dominated by regions where two of the three momentum fractions vanish. The convolution over $dx_1 dx_2 dx_3$ in Eq. (2) is simplified to an integration over only one momentum fraction,

$$\begin{aligned} &\int \prod_{i=1}^3 dx_i T_{(jj')/p_A}(\{x_i\}) \hat{\sigma}_{(jj')}^{(4)}(\{x_i\}p) \\ &\Rightarrow \int dx T_q(x, A) \hat{\sigma}_q^{(D)}(xp), \end{aligned} \quad (4)$$

where the partonic part $\hat{\sigma}^{(D)}$ is finite and perturbative, with the superscript (D) indicating the contribution from

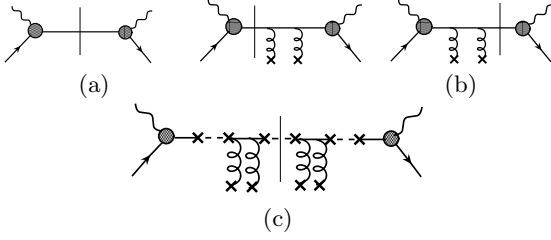


Fig. 4. Tree diagrams give to the leading medium-size enhanced contributions to DIS cross sections.

double scattering. The above matrix element, $T_q(x, A)$, as illustrated in Fig. 3(b), has the form

$$T_q(x, A) = \int \frac{dy_1^-}{2\pi} e^{ip^+ xy_1^-} \int \frac{dy_2^- dy_3^-}{2\pi} \theta(y_2^- - y_1^-) \theta(y_3^-) \times \frac{1}{2} \langle p_A | \bar{q}(0) \gamma^+ F^{\alpha+}(y_3^-) F^-_{\alpha}(y_2^-) q(y_1^-) | p_A \rangle \quad (5)$$

where $|p_A\rangle$ is the relevant nuclear state. The variable x here is the fractional momentum associated with the hard parton from the target that initiates the process. Similar gluon-gluon correlation function $T_g(x, A)$ is also important [16]. In this type of the twist-4 parton-parton correlation functions, two integrals over the y^- and y_2^- can grow with the nuclear radius. However, if we require local color confinement, the difference between the light-cone coordinates of the two field strengths should be limited to the nucleon size and only one of the two y_i^- integrals can be extended to the size of nuclear target. The twist-4 parton-parton correlation functions are then proportional to the size of the target, that is, enhanced by $A^{1/3}$.

It is important to emphasize that using a pole in the complex x_i (longitudinal momentum) space to do the integral does not assume on-shell propagation for the scattered quark. Indeed, the x_i integrals are not pinched between coalescing singularities at such points, and the same results could be derived by performing the x_i integrals without going through the $x_i = 0$ points [2].

3 Coherent power corrections in DIS

The inclusive DIS cross section on a nucleus provides an unique probe for effects of *coherent* multiple scatterings by varying the value of Bjorken x_B . Under the approximation of one-photon exchange, the unpolarized inclusive DIS cross section probes two structure functions: $F_T(x_B, Q^2)$ and $F_L(x_B, Q^2)$, corresponding to the transverse and longitudinal polarization states of the virtual photon, respectively [17, 18]. The structure functions at the lowest order in α_s are given by [17]

$$F_T^{(LT)}(x_B, Q^2) = \frac{1}{2} \sum_q e_q^2 q(x_B, Q^2) + \mathcal{O}(\alpha_s), \quad (6)$$

$$F_L^{(LT)}(x_B, Q^2) = \mathcal{O}(\alpha_s), \quad (7)$$

where (LT) indicates the leading twist contribution – the first row in Eq. (1), \sum_q runs over the (anti)quark flavors,

e_q is their fractional charge, and $q(x, Q^2)$ is the leading twist quark distribution:

$$q(x, Q^2) = \int \frac{dy^-}{2\pi} e^{ixp^+ y^-} \langle p | \bar{q}(0) \frac{\gamma^+}{2} q(y^-) | p \rangle \quad (8)$$

in the lightcone $A^+ = n^\mu A_\mu = 0$ gauge for hadron momentum $p^\mu = p^+ \bar{n}^\mu$ with $\bar{n}^\mu = [1, 0, 0_\perp]$ and $n^\mu = [0, 1, 0_\perp]$.

The Feynman diagrams in Fig. 4 give the leading tree level contributions to the lepton-nucleus DIS cross section. The cut-line represents the final state [3]. For transversely polarized photons Fig. 4(a) gives the leading twist partonic contribution,

$$d\hat{\sigma}_T^{(0)} = \frac{1}{2} e_q^2 \delta(x - x_B), \quad (9)$$

from which $F_T^{(LT)}$ in Eq. (6) is derived after convoluting with the leading twist quark distribution in Eq. (8). Diagrams with two gluons in Fig. 4(b) gives the first power correction to transverse partonic cross section [3, 18],

$$d\hat{\sigma}_T^{(1)} = \frac{1}{2} e_q^2 \left[\frac{1}{2N_c} \right] \frac{g^2}{Q^2} \left[2\pi^2 \tilde{F}^2(0) \right] x_B \left[-\frac{d}{dx} \delta(x - x_B) \right] \quad (10)$$

with the two-gluon field operator

$$\left[\tilde{F}^2(0) \right] = \int \frac{dy_2^- dy_1^-}{(2\pi)^2} \left[F^{+\alpha}(y_2^-) F_{\alpha}^+(y_1^-) \right] \theta(y_2^-); \quad (11)$$

and the first power correction to transverse structure function [3, 18],

$$F_T^{(1)}(x_B, Q^2) = \left[\frac{4\pi^2 \alpha_s}{Q^2} \left(\frac{1}{2N_c} \right) \right] \times \frac{1}{2} \sum_q e_q^2 x_B \frac{d}{dx_B} T_q(x_B, A) \quad (12)$$

with correlation function, $T_q(x_B, A)$, given in Eq. (5).

The four-parton correlation functions T_q 's are nonperturbative and must be taken from experiments. To estimate the magnitude of T_q 's, we could choose a simple ansatz [19]

$$T_i(x, A) = \lambda^2 A^{1/3} \phi_{i/p_A}(x, A) \quad (13)$$

for $i = q, g$ in terms of the corresponding twist-2 effective nuclear parton distribution $\phi_{i/A}$. We choose this form because we expect the x -dependence of the probability to detect the hard parton to be essentially unaffected by the presence or absence of an additional soft scattering. In Eq. (13) λ is assumed to be a constant with dimensions of mass. This ansatz facilitates the comparison to data [2].

If we further assume that a nucleus is made of a group of loosely bound color singlet nucleons, packed in a hard sphere of radius $RA^{1/3}$, we can approximate the matrix element of nuclear state in Eq. (5) into a product of matrix elements of nucleon states [3, 20],

$$\begin{aligned} & \langle p_A | \bar{q}(0) \frac{\gamma^+}{2} \left[\tilde{F}^2(0) \right] q(y^-) | p_A \rangle \\ & \approx \frac{A}{2\pi} \left[\frac{\frac{3}{4} RA^{1/3}}{\frac{1}{\frac{4\pi}{3} R^3}} \right] \langle F^{+\alpha} F_{\alpha}^+ \rangle \langle p | \bar{q}(0) \frac{\gamma^+}{2} q(y^-) | p \rangle \end{aligned} \quad (14)$$

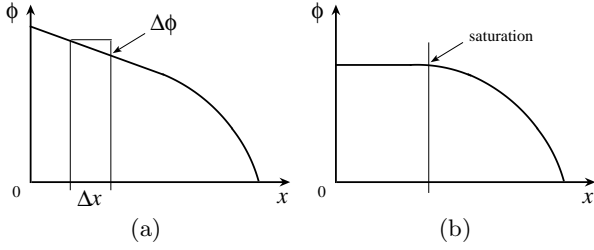


Fig. 5. Sketch for the x -dependence of normal (a) and saturated (b) parton distributions.

with $p = p_A/A$ and the two-gluon matrix element [3]

$$\langle F^{+\alpha} F_{\alpha}^{+} \rangle \equiv \frac{1}{p^{+}} \int \frac{dy^{-}}{2\pi} \langle p | F^{+\alpha}(0) F_{\alpha}^{+}(y^{-}) | p \rangle \theta(y^{-}). \quad (15)$$

Substituting Eq. (15) into the definition of quark-gluon correlation function, $T_q(x, A)$ in Eq. (5), we drive

$$\lambda^2 \approx \left(\frac{3}{4} R \right) \left(\frac{1}{\frac{4\pi}{3} R^3} \right) \langle F^{+\alpha} F_{\alpha}^{+} \rangle, \quad (16)$$

and

$$F_T^{(1)}(x_B, Q^2) \approx \frac{3\pi\alpha_s}{8Q^2 R^2} \langle F^{+\alpha} F_{\alpha}^{+} \rangle (A^{1/3} - 1) \times \frac{1}{2} \sum_q e_q^2 x_B \frac{d}{dx_B} q_A(x_B, Q^2) \quad (17)$$

where q_A defined in Eq. (8) with $p = p_A/A$. In deriving Eq. (17), we used $A^{1/3} - 1$ instead of $A^{1/3}$ for the line integral between the two pairs of field operators in Eq. (15) so that the nuclear effect vanishes for $A = 1$ [3]. From Eq. (17) and known generic x -dependence of parton distributions, as sketched in Fig. 5(a), the leading coherent power correction *suppresses* the DIS cross section or structure functions at small x_B .

If x_B is small enough, the virtual photon could interact *coherently* with all nucleons inside a large nucleus. From the Feynman diagrams in Fig. 4(c) with $2N$ gluons, we derive the leading N th coherent power corrections to the transverse structure function [3],

$$F_T^{(N)}(x_B, Q^2) = \left[\frac{3\pi\alpha_s}{8Q^2 R^2} \langle F^{+\alpha} F_{\alpha}^{+} \rangle (A^{1/3} - 1) \right]^N \times \frac{1}{2} \sum_q e_q^2 \frac{1}{N!} x_B^N \frac{d^N}{dx_B^N} q_A(x_B, Q^2). \quad (18)$$

Summing over all leading $A^{1/3}$ -enhanced power corrections, the first column of the right-hand-side of Eq. (1), we obtain [3]

$$F_T^A(x_B, Q^2) = \sum_{n=0}^N \frac{1}{n!} \left[\frac{\xi^2}{Q^2} (A^{1/3} - 1) \right]^n \times x_B^n \frac{d^n}{dx_B^n} F_T^{A(LT)}(x_B, Q^2) \quad (19)$$

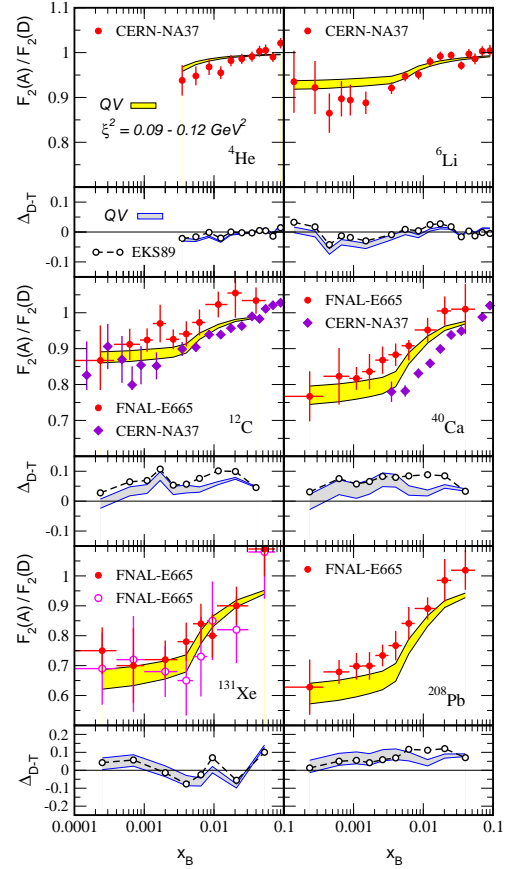


Fig. 6. From [3], all-twist resummed $F_2(A)/F_2(D)$ calculation versus DIS data on nuclei [25]. Data-Theory Δ_{D-T} is also shown.

with a characteristic scale of the power corrections

$$\xi^2 \equiv \frac{3\pi\alpha_s}{8R^2} \langle F^{+\alpha} F_{\alpha}^{+} \rangle. \quad (20)$$

If we approximate $N \sim \infty$ in Eq. (19), we obtain,

$$F_T^A(x_B, Q^2) \approx F_T^{A(LT)}(x_B(1 + \Delta), Q^2) \quad (21)$$

with $\Delta \equiv (A^{1/3} - 1) \xi^2 / Q^2$, a shift in x_B . Similar expression was derived for the longitudinal structure function $F_L^A(x_B, Q^2)$ [3].

With only one unknown matrix element, $\langle F^{+\alpha} F_{\alpha}^{+} \rangle$, our calculated results can be easily tested and challenged. From Eq. (21), the nuclear dependence in structure functions should come from two distinctive sources: universal A -dependence in leading twist parton distributions and process sensitive A -dependence from power corrections [2, 3]. By comparing our numerical results, evaluated with CTEQ6 PDFs [21], with the data, we extract the *maximum* size of power corrections. For $\xi^2 = 0.09 - 0.12 \text{ GeV}^2$, our calculated reduction in nuclear structure functions is consistent with the x_B -, Q^2 - and A -dependence of the data as demonstrated Fig. 6.

The predictive power of factorization approach resides in the universality of unknown matrix elements. Without

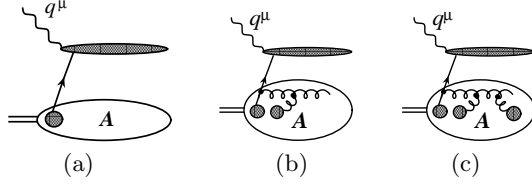


Fig. 7. Sample DIS diagrams have initial-state collinear divergence involving parton recombinations.

additional unknown matrix elements, our predictions for neutrino DIS cross section on an iron target are consistent with NuTeV data [22, 23]. At small and moderate Q^2 , our prediction gives a very good description of SLAC E143 data on $R = \sigma_L/\sigma_T$ of ^{12}C target [3, 24]

The resummed power correction has a nontrivial dependence on the target A and kinematic variables x_B and Q^2 because its connection to the x -dependence of the active parton distribution. The effect disappears if the parton distribution is saturated at a very small x , as sketched in Fig. 5(b). The leading power correction calculated here is a consequence of the limited phase space in a given collision. If we would integrate over x_B from $-\infty$ (or zero) to ∞ for a purely inclusive process (or a process with an infinite collision energy), the $F_T^{(N)}$ vanishes for $N \neq 0$ due to the unitarity condition [8].

QCD factorization systematically moves all collinear divergences from partonic scattering into long-distance matrix elements. At the leading power, DGLAP evolved parton distributions are sufficient to absorb all collinear divergences in γ^* -parton scattering cross section to ensure the infra-safety of all coefficient functions in the first row of Eq. (1). However, DGLAP evolved parton distributions do not remove collinear divergences involving multiple parton recombination, like those in Fig. 7(b) and (c). A modified evolution equation taking into account the parton recombination slows down the fast growth of parton density at small x [20, 26], and keeps a positive density of small- x gluons at low Q^2 [27]. All order resummed power corrections – coherent parton recombinations to parton evolution should be very valuable for approaching the region of parton saturation from the perturbative side and for getting a reliable picture of small- x partons [28, 29].

4 Power correction to Drell-Yan cross section

It was shown by the NA38 and NA50 Collaborations that muon pair production for dimuon invariant mass between ϕ and J/ψ , known as the intermediate mass region (IMR), in heavy nucleus-nucleus collisions exceeds the expectation based on a linear extrapolation of the $p - A$ sources with the product of the mass numbers of the projectile and target nuclei [30]. The excess increases with the number of participant nucleons, and the ratio between the observed dimuon yield and the expected sources reaches a factor of 2 for central Pb-Pb collisions. There have been a lot of effort to attribute such an excess to the enhancement

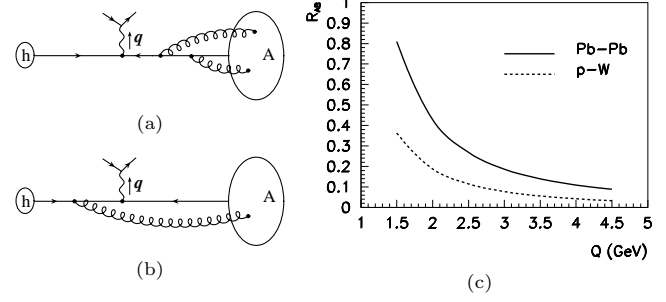


Fig. 8. Sketch for Drell-Yan process in hadron-nucleus collision with multiple interactions internal to nucleus (a) and sensitive to hard scattering (b); and the nuclear modification factor, $R_{AB}(Q)$, as a function of dilepton mass Q .

of open charm production [31], thermal dimuons production [32], and secondary meson-meson scattering in nuclear medium [33]. As shown in Ref. [30], the Drell-Yan continuum is the dominant source of the dilepton production in this mass range. An enhancement in the Drell-Yan continuum is much more effective than all other sources for interpreting the observed excess.

In hadron-nucleus and nucleus-nucleus collisions, more partons are available at a given impact parameter. Before the hard collision of producing the lepton-pair, partons from different nucleons can either interact between themselves, as sketched in Fig. 8(a) which leads to the universal nuclear dependence in parton distributions, or interact with the incoming parton, as sketched in Fig. 8(b) which gives the medium-size enhanced power corrections [34]. For the kinematics of IMR Drell-Yan process, parton distributions have a weak nuclear dependence and produce a small reduction to the cross section. On the other hand, the medium size enhanced power corrections are process dependent, and actually *increase* the production rate and become more important when Q^2 decreases [34]. Let inclusive Drell-Yan cross section in nuclear collisions be approximated as

$$\begin{aligned} \frac{d\sigma_{AB}}{dQ^2} &\approx AB \frac{d\sigma_{NN}^{(S)}}{dQ^2} + \frac{d\sigma_{AB}^{(D)}}{dQ^2} + \dots \\ &\equiv AB \frac{d\sigma_{NN}^{(S)}}{dQ^2} [1 + R_{AB}(Q)] , \end{aligned} \quad (22)$$

where superscripts (S) and (D) represent the single and double scattering, respectively. The $R_{AB}(Q)$ defines a nuclear modification factor of Drell-Yan continuum. Fig. 8(c) shows the calculated $R_{AB}(Q)$ from medium-size enhanced double scattering [34]. In evaluating Fig. 8(c), we used the same quark-gluon correlation function, $T_q(x, A)$, and neglected the A -dependence in parton distributions. Therefore, we expect that the true enhancement to the Drell-Yan continuum might be slightly smaller than $R_{AB}(Q)$ in Fig. 8(c), which is a very significant effect.

It is perhaps surprising that the medium-size enhanced power correction to DIS and Drell-Yan cross sections carries a different sign. The sign difference is a consequence of the kinematic nature of the calculated leading power

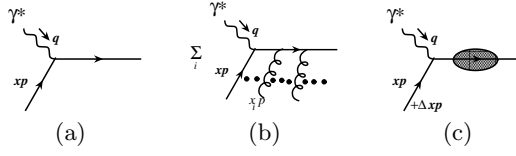


Fig. 9. DIS with a space-like hard scale

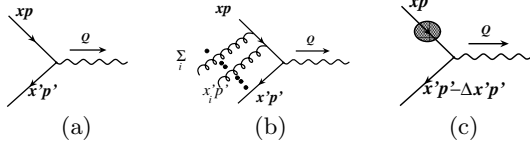


Fig. 10. Drell-Yan with a time-like hard scale

corrections. The sketch in Fig. 9 shows that the sum of multiple soft rescattering to the final-state parton in DIS effectively broadens the parton's transverse momentum [35] (or gives the parton an effective mass [22]); and the on-shell condition of the final-state parton forces an extra momentum fraction Δxp to the incoming parton. On the other hand, the multiple initial-state soft rescattering in Drell-Yan process *broadens* the incoming parton's momentum, and the kinematics (or the measured q^μ) of the observed dilepton pair forces the active parton from the target to take away some of its momentum, a negative shift in momentum fraction, as shown in Fig. 10(c).

5 Transverse momentum Q_T broadening

Coherent multiple rescatterings not only modify the production rate of inclusive cross sections, but also affect the momentum distribution of produced particles. Although the amount of broadening due to each soft rescattering is too weak a scale to warrant a reliable calculation, an averaged broadening in a hard collision could be a physical quantity calculable in pQCD [2].

In Ref. [35], Drell-Yan transverse momentum broadening was calculated in pQCD by evaluating the lowest order soft rescattering diagram in Fig. 11(a). Although the direct Q_T modification from soft rescattering to $d\sigma/dQ^2 dQ_T^2$ is not perturbatively calculable because of the size of small Q_T kick, the Q_T broadening,

$$\langle Q_T^2 \rangle \equiv \int dQ_T^2 Q_T^2 \frac{d\sigma}{dQ^2 dQ_T^2} \bigg/ \int dQ_T^2 \frac{d\sigma}{dQ^2 dQ_T^2}, \quad (23)$$

is calculable [2, 8]. It was found that the Drell-Yan transverse momentum broadening in hadron-nucleus collisions can be expressed in terms of the same quark-gluon correlation function $T_q(x, A)$ (not its derivative) [35],

$$\langle Q_T^2 \rangle \approx \left(\frac{4\pi^2 \alpha_s}{3} \right) \frac{\sum_q e_q^2 \int dx' f_{\bar{q}/h}(x') T_q(\tau/x', A)/x'}{\sum_q e_q^2 \int dx' f_{\bar{q}/h}(x') f_q(\tau/x', A)/x'} \quad (24)$$

where \sum_q runs over all quark and antiquark flavors, e_q is the quark fractional charge, and $\tau = Q^2/s$, in terms of the

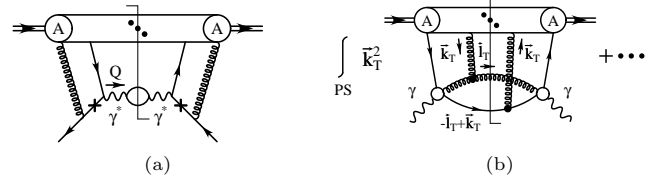


Fig. 11. (a) Lowest order diagram that contributes to the Drell-Yan transverse momentum broadening in hadron-nucleus collisions; (b) Sketch for the lowest order contributions to the averaged di-jet momentum imbalance in photoproduction.

lepton-pair invariant mass Q and hadron-hadron center of mass energy, \sqrt{s} .

Adopting the model in Eq. (13), the lowest order Drell-Yan transverse momentum broadening in Eq. (24) can be simplified as

$$\langle Q_T^2 \rangle_{4/3} = \left(\frac{4\pi^2 \alpha_s}{3} \right) \lambda^2 A^{1/3}. \quad (25)$$

By comparing Eq. (25) to data from Fermilab E772 and CERN NA10 experiments [36, 37], it was found [35] that $\lambda_{DY}^2 \sim 0.01 \text{ GeV}^2$, which corresponds to $\xi_{DY}^2 \sim 0.04 \text{ GeV}^2$ that is about a factor of 2 *smaller* from what was extracted from inclusive DIS data, where the leading twist nuclear dependence was not included. The difference might be caused by the difference between initial-state and final-state rescattering effects [2].

Momentum imbalance between two final-state jets in photoproduction off a nuclear target was calculated by evaluating the diagrams like one in Fig. 11(b), and was compared with Fermilab E683 data [19], with an assumption that the momentum imbalance between two jets is approximately the same as the momentum imbalance between two final-state partons. Again, the calculated momentum imbalance was expressed in terms of the same quark-gluon and gluon-gluon correlation function [19]. By comparing with the momentum imbalance data for jet transverse momentum $p_T > 4 \text{ GeV}$ [38], it was found [19] that $\lambda_{\text{dijet}}^2 = 0.05 - 0.1 \text{ GeV}^2$, which corresponds to $\xi^2 \sim 0.2 \text{ GeV}^2$ that is about a factor 2 *bigger* than what was found in DIS. As pointed out in Ref. [2], high order corrections to initial-state and final-state soft rescattering could be very different and significantly reduce the difference of the nonperturbative parameter.

6 Nuclear suppression in hadron-nucleus collisions

Dynamical nuclear effects induced by soft rescattering can be studied through the ratio of particle production rates in hadron-nucleus and hadron-hadron collisions. However, there is no observed variable, like x_B in inclusive DIS, that can directly measure the coherence length of the hard scattering. All incoming parton momentum fractions are convoluted over, and strength of the collision is measured by Lorentz invariants, like Mandelstam variables, \hat{s} ,

\hat{t} , and \hat{u} . Unlike in DIS and in Drell-Yan, there are both initial-state and final-state soft rescattering in hadronic collisions, which could in principle lead to medium size enhanced power corrections. Since the hard scales, \hat{s} , \hat{t} , and \hat{u} , in hadronic collisions are often much larger than a couple of GeV^2 , effect of the medium size enhanced power corrections to hard probes in hadronic collisions is in general less significant. However, in the most forward (backward) region, the invariant \hat{t} (\hat{u}) could be much smaller than the other invariants, so that the power corrections in $1/\hat{t}$ ($1/\hat{u}$) could become very important [14].

Consider, for example, the single hadron inclusive production in hadron-nucleus collision as shown in Fig. 2(b). Once we fix the momentum fractions x_a and z_1 , the effective interaction region is determined by the momentum exchange $q^\mu = (x_a P_a - P_c/z_1)^\mu$. In the head-on frame of $q - P_b$, the scattered parton of momentum ℓ interacts coherently with partons from different nucleons at the same impact parameter, just like that in DIS. Interactions that take place between the partons from the nucleus and the incoming parton of momentum $x_a P_a$ and/or the outgoing parton of momentum P_c/z_1 at a different impact parameter are much less coherent and actually dominated by the independent elastic scattering [39]. Similar to the DIS case [11], we find [14] that resumming the coherent scattering with multiple nucleons is equivalent to a shift of the momentum fraction of the active parton from the nucleus in Fig. 2(b),

$$x_b \rightarrow x_b \left(1 + \frac{C_d \xi^2 (A^{1/3} - 1)}{(-\hat{t})} \right), \quad (26)$$

with the hard scale $\hat{t} = q^2 = (x_a P_a - P_c/z_1)^2$ and the color factor C_d depending on the flavor of parton d . $C_q(\bar{q}) = 1$ and $C_g = C_A/C_F = 9/4$ for quark (antiquark) and gluon, respectively. The shift in Eq. (26) leads to a net suppression of the cross sections, and the \hat{t} -dependence of this shift indicates that the attenuation increases in the forward rapidity region.

The top panels of Fig. 12 show the rapidity and transverse momentum dependence of $R_{dAu}^{h_1}(b)$ and $R_{dAu}^{h_1 h_2}(b)$, the ratio of single and double hadron production, respectively, in minimum bias $d+Au$ collisions. The amplification of the suppression effect at forward y_1 comes from the steepening of the parton distribution functions at small x_b and the decrease of the Mandelstam variable $(-\hat{t})$. At high p_{T1}, p_{T2} the attenuation is found to disappear in accord with the QCD factorization theorems [40]. The bottom panels of Fig. 12 show the growth of the nuclear attenuation effect with centrality.

Dihadron correlations $C_2(\Delta\varphi) = \frac{1}{N_{\text{trig}}} \frac{dN_{\text{dijet}}^{h_1 h_2}}{d\Delta\varphi}$ associated with $2 \rightarrow 2$ partonic hard scattering processes, after subtracting the bulk many-body collision background, can be approximated by near-side and away-side Gaussians. The acoplanarity, $\Delta\varphi \neq \pi$, arises from high order QCD corrections and in the presence of nuclear matter - transverse momentum diffusion [39]. If the strength of the away-side correlation function in elementary N+N collisions is normalized to unity, dynamical quark and gluon

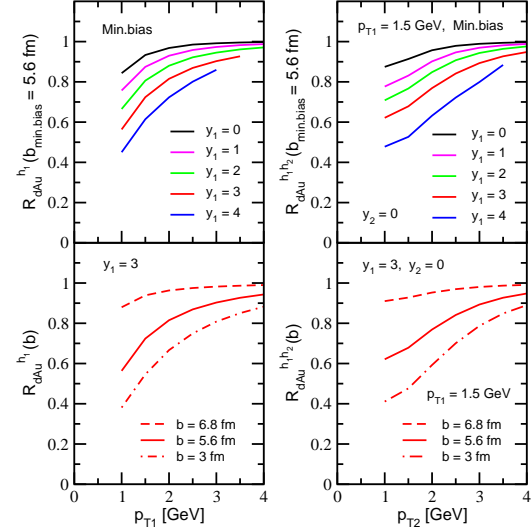


Fig. 12. From [14]. Suppression of the single and double inclusive hadron production rates as a function of p_T in $d + Au$ collisions at $\sqrt{s} = 200 \text{ GeV}^2$ at different rapidities (Top) and at different impact parameters (Bottom). The trigger hadron p_{T1}

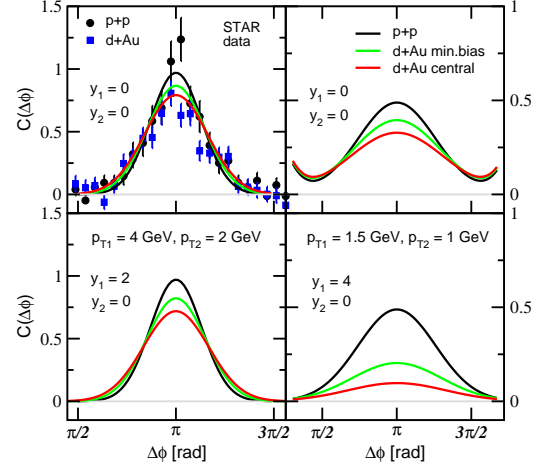


Fig. 13. From [14]. Centrality dependence of $C_2(\Delta\varphi)$ at various rapidities and moderate (left) and small (right) transverse momenta. Central $d + Au$ and $p + p$ data from STAR [43].

shadowing in $p + A$ reactions will be manifest in the attenuation of the area $A_{\text{Far}} = R_{pA}^{h_1 h_2}(b)$ [14].

The left panels of Fig. 13 show that for $p_{T1} = 4 \text{ GeV}$, $p_{T2} = 2 \text{ GeV}$ the dominant effect in $C_2(\Delta\varphi)$ is a small increase of the broadening with centrality, compatible with the PHENIX[42] and STAR[43] measurements. Even at forward rapidity, such as $y_1 = 2$, the effect of power corrections in this transverse momentum range is not very significant. At small $p_{T1} = 1.5 \text{ GeV}$, $p_{T2} = 1 \text{ GeV}$, shown in the right hand side of Fig. 13, the apparent width of the away-side $C_2(\Delta\varphi)$ is larger. In going from midrapidity, $y_1 = y_2 = 0$, to forward rapidity, $y_1 = 4, y_2 = 0$, we find a significant reduction by a factor of 3 - 4 in the strength of

dihadron correlations. Preliminary STAR results [44] are consistent with our predictions.

7 Summary and outlook

We have briefly reviewed a pQCD factorization approach to coherent multiple scattering and argued that the $A^{1/3}$ -type medium size enhanced power corrections caused by multiple soft rescattering can be consistently calculated in pQCD. We presented calculations of rescattering effects in inclusive cross sections as well as transverse momentum broadening (or the moment of particle transverse momentum distributions.). By studying the coherent multiple scattering, we can probe new sets of fundamental and universal multiparton correlation functions in nuclear medium. These new functions provide new insights into the nonperturbative regime of QCD.

Initial pQCD calculations of multiple rescattering effects is very successful in understanding nuclear dependence of inclusive cross sections. For a wide range of observables, the estimate for the only unknown parameter is reasonably consistent. With a single unknown parameter, the calculations describe many observables and their nuclear dependences fairly well. The factorization approach, with its intuitive and transparent results, can be easily applied to study the nuclear modification of other physical observables in $p + A$ reactions. The systematic incorporation of coherent power corrections provides a novel tool to address the most interesting transition region between “hard” and “soft” physics in hadron-nucleus collisions.

This work is supported in part by the U.S. Department of Energy under Grant No. DE-FG02-87ER40371.

References

1. CERN Yellow Report (CERN-2004-009 on “Hard probes in heavy-ion collisions at the LHC”, edited by M. Mangano, H. Satz, and U. Wiedemann (Geneva, Switzerland, 2004), and references therein.
2. J. W. Qiu and G. Sterman, Int. J. Mod. Phys. E **12** (2003) 149 [arXiv:hep-ph/0111002].
3. J. W. Qiu and I. Vitev, arXiv:hep-ph/0410218.
4. R. Baier, Y. L. Dokshitzer, A. H. Mueller, S. Peigne and D. Schiff, Nucl. Phys. B **483** (1997) 291 [arXiv:hep-ph/9607355]; Nucl. Phys. B **484** (1997) 265 [arXiv:hep-ph/9608322].
5. B.G. Zakharov, JETP Lett. **70** (1999) 176; R. Baier, D. Schiff and B. G. Zakharov, Ann. Rev. Nucl. Part. Sci. **50** (2000) 37 [arXiv:hep-ph/0002198].
6. M. Gyulassy, P. Levai and I. Vitev, Nucl. Phys. B **594** (2001) 371, and references therein.
7. X. F. Guo and X. N. Wang, Phys. Rev. Lett. **85** (2000) 3591; X. N. Wang and X. F. Guo, Nucl. Phys. A **696** (2001) 788.
8. J. W. Qiu and G. Sterman, Nucl. Phys. B **353** (1991) 137.
9. J. W. Qiu, Nucl. Phys. A **715** (2003) 309 [arXiv:nucl-th/0211086].
10. J. W. Qiu, in CERN Yellow Report (CERN-2004-009 on “Hard probes in heavy-ion collisions at the LHC”, edited by M. Mangano, H. Satz, and U. Wiedemann (Geneva, Switzerland, 2004), PP14 [arXiv:hep-ph/0305161].
11. J. W. Qiu and I. Vitev, Phys. Rev. Lett. **93** (2004) 262301 [arXiv:hep-ph/0309094].
12. R. L. Jaffe and M. Soldate, Phys. Lett. B **105** (1981) 467; Phys. Rev. D **26** (1982) 49.
13. J. W. Qiu and G. Sterman, Nucl. Phys. B **353** (1991) 105.
14. J. W. Qiu and I. Vitev, arXiv:hep-ph/0405068.
15. K.G. Wilson, Phys. Rev. **179** (1969) 1499.
16. M. Luo, J. W. Qiu and G. Sterman, Phys. Lett. B **279** (1992) 377; Phys. Rev. D **50** (1994) 1951.
17. R. Brock *et al.*, Rev. Mod. Phys. **67**, 157 (1995).
18. X. F. Guo, J. W. Qiu and W. Zhu, Phys. Lett. B **523** (2001) 88 [arXiv:hep-ph/0110038].
19. M. Luo, J. W. Qiu and G. Sterman, Phys. Rev. D **49** (1994) 4493.
20. A. H. Mueller and J. W. Qiu, Nucl. Phys. B **268** (1986) 427.
21. J. Pumplin *et al.*, JHEP **0207**, 012 (2002).
22. J. W. Qiu and I. Vitev, Phys. Lett. B **587** (2004) 52 [arXiv:hep-ph/0401062].
23. I. Vitev, arXiv:hep-ph/0506039.
24. K. Abe *et al.*, Phys. Lett. B **452**, 194 (1999).
25. M. Arneodo *et al.*, Nucl. Phys. B **441**, 12 (1995); P. Amaudruz *et al.*, Nucl. Phys. B **441**, 3 (1995); M.R. Adams *et al.*, Z. Phys. C **67**, 403 (1995); Phys. Rev. Lett. **68**, 3266 (1992).
26. L. V. Gribov, E. M. Levin and M. G. Ryskin, Phys. Rept. **100** (1983) 1.
27. K. J. Eskola, H. Honkanen, V. J. Kolhinen, J. w. Qiu and C. A. Salgado, arXiv:hep-ph/0302185.
28. W. Zhu, Nucl. Phys. A **753** (2005) 206 [arXiv:hep-ph/0408328].
29. J. W. Qiu and Z. Kang, in preparation.
30. M.C. Abreu *et al.*, NA38 and NA50 Collaborations, Eur. Phys. J. **C14**, 443 (2000).
31. C. Y. Wong and Z. Q. Wang, Phys. Lett. B **367**, 50 (1996).
32. R. Rapp and E. Shuryak, Phys. Lett. B **473**, 13 (2000).
33. Z. Lin and X. N. Wang, Phys. Lett. B **444**, 245 (1998).
34. J. W. Qiu and X. Zhang, Phys. Lett. B **525** (2002) 265 [arXiv:hep-ph/0109210].
35. X. Guo, Phys. Rev. D **58** (1998) 114033. [hep-ph/9804234].
36. D. M. Alde *et al.*, E772 Collaboration, Phys. Rev. Lett. **64**, 2479 (1990).
37. P. Bordale, *et al.*, NA 10 Collaboration, Phys. Lett. B **193** (1987) 373.
38. D. Naples *et al.* (E683 Collaboration) Phys. Rev. Lett. **72** (1994) 2341.
39. M. Gyulassy, P. Levai and I. Vitev, Phys. Rev. D **66**, 014005 (2002); J. W. Qiu, I. Vitev, Phys. Lett. B **570**, 161 (2003); I. Vitev, Phys. Lett. B **562**, 36 (2003).
40. J. C. Collins, D. E. Soper and G. Sterman, Adv. Ser. Direct. High Energy Phys. **5** (1988) 1 [arXiv:hep-ph/0409313].
41. I. Vitev, J. Phys. G **31** (2005) S557 [arXiv:hep-ph/0409297].
42. J. Rak, J. Phys. G **30**, S1309 (2004); K. Filimonov, J. Phys. G **30**, S919 (2004).
43. J. Adams *et al.*, Phys. Rev. Lett. **91**, 072304 (2003).
44. A. Ogawa, nucl-ex/0408004.

